Glass Transition and Melting Behavior of Poly(oxy-1,4-phenyleneoxy-1,4-phenylenecarbonyl-1,4-phenylene)

Stephen Z. D. Cheng, M.-Y. Cao, and Bernhard Wunderlich*

Department of Chemistry, Rensselaer Polytechnic Institute, Troy, New York 12181-3590.
Received March 3, 1986; Revised Manuscript Received April 18, 1986

ABSTRACT: Thermal analysis of typical poly(oxy-1,4-phenyleneoxy-1,4-phenylenecarbonyl-1,4-phenylene) (PEEK) has been carried out from 130 to 650 K for samples variously crystallized between 593 and 463 K or quenched to the glassy state. The heat capacity, C_p, is crystallinity independent to 240 K. Between 240 K and the glass transition temperature T_g (419–430 K depending on crystallization conditions) the amorphous solid has a slightly higher C_p. Above T_g poorly crystallized samples show a rigid-amorphous fraction that does not contribute to the increase in C_p at T_g. Crystallinity reduces the heat capacity hysteresis at T_g. On crystallization three types of crystallinity must be distinguished: w^c(H), w^c(L), and w^c(C). Fusion peaks at high and low temperatures characterize w^c(H) and w^c(L), respectively; w^c(C) forms on cooling after crystallization and causes an increase in C_p starting at about 460 K. The metastability, sequence of crystallization, recrystallization, and reorganization on analysis by heating at a constant rate and on stepwise crystallization are analyzed.

Introduction

High-temperature polymers containing phenylene groups are increasingly interesting as thermoplastic matrix materials in composites for engineering purposes. Poly(oxy-1,4-phenyleneoxy-1,4-phenylenecarbonyl-1,4-phenylene) [poly(aryl ether ether ketone) or PEEK] is one of them. It is a semicrystalline polymer with an unusual combination of properties, such as high chemical resistance, excellent thermal stability, and good mechanical properties.

Previous studies of PEEK focused in our laboratory on the representation of its heat capacity in the solid state in terms of its vibrational frequency spectrum.[1] The thermodynamics of its liquid state was also analyzed[2] before. At the glass transition temperature, 419 K, the heat capacity increases by 78.1 J K^{-1} mol^{-1}.[1,2] The equilibrium melting temperature, 668 K, and its heat of fusion for hypothetical 100% crystallinity, 37.5 kJ/mol per repeating unit (mass 288.3 g), were reported by others earlier.[3] A typical differential scanning calorimeter (DSC) curve of quenched PEEK is shown in Figure 1. The glass transition, crystallization exotherm, and melting endotherm are clearly shown.

Other properties have also been studied recently. The PEEK crystal structure[4–6] and morphology[7,8] are known. Solution properties and molecular weight determinations[9,10] have been reported.

This paper presents a study of the thermal analysis of semicrystalline PEEK of various crystallinity. Special attention is paid to the heat capacity in the temperature region 200 K to T_g, where possible local motion in the amorphous state could cause an increase in heat capacity, as found, for example, earlier for polyethylene.[11] The nature of the glass transition itself is commonly changing with degree of crystallization. Its temperature may shift, its hysteresis behavior may be different, and there may be a morphology-dependent rigid-amorphous fraction (causing a lower heat capacity). The rigid-amorphous fraction unfreezes at a higher temperature only, as was found, for example, in poly(oxymethylene).[12] Finally, all semicrystalline polymers show below the main melting range an increase in heat capacity or premelting peaks due to morphology-dependent defect reorganization, crystal reorganization, annealing, or premelting.[13] The single or multiple melting peaks in themselves can be used for interpretation of polymer crystal domain size, melting kinetics, and crystal reorganization, in addition to the determination of melting temperature and crystallinity.[13]

Once the thermal characteristics of a macromolecule are established, thermal analysis is a valuable tool for quality control and assessment of thermal history.[14]

Experimental Section

Materials and Samples. The PEEK for our research was produced by ICI Co., no additional information had been provided. From the thermal properties, the PEEK sample we used can be judged closely similar to those of Blundell and Osborn.[3] DSC samples of PEEK were prepared in aluminum pans. The sample weight was over 20 mg in order to obtain precise heat capacity measurements. All samples were selected for uniform thickness, smooth sample surfaces, and constant shape. The sample weights were recorded to ±0.001 mg.

Equipment and Experiments. All samples were measured with either a Perkin-Elmer DSC2 or a Perkin-Elmer DSC4. Four temperature ranges were selected for measurement: 130–250, 220–380, 325–500, and 400–650 K. The DSC was calibrated in these four temperature ranges following the standard procedure.[15] Both temperature and heat flow scales were corrected with standard chemical materials (*n*-heptane, *n*-octane, *n*-decane, *n*-dodecane, naphthalene, benzoic acid, indium, tin, lead, and zinc). For the measurement of heat capacity, the base lines of the empty pan and Al_2O_3 (sapphire) reference were measured and compared to the heat flow measurements of the PEEK samples. All pan weights were kept within ±0.002 mg. The repeatability of our Al_2O_3 heat capability measurements, based on the data of the National Bureau of Standards,[16] was within ±0.1%.

For isothermal crystallization from the melt, the samples were first heated to 680 K and held about 2 min, to obtain a crystal-free melt, and then cooled to the crystallization temperature, T_c, and kept for the crystallization time, t_c. The lowest T_c still permitted thermal equilibration before a noticeable exotherm developed. The isothermal crystallization was followed by cooling at a rate of −0.31 K/min and analysis by heating or by direct analysis without prior cooling to lower temperature. The analyses were recorded at 10 K/min extending to 650 K.

For isothermal crystallization from the glassy state, the samples were heated to 680 K and held for 2 min, as before. Then, the samples were quenched in liquid N_2 to make totally amorphous samples. Different crystallization temperatures, T_c, were chosen for isothermal crystallization, and the samples were heated from below T_g to T_c at 320 K/min. The crystallization time t_c was counted from attainment of T_c. For analysis, the same procedures (with and without cooling) were used, as in the case of crystallization from the melt. Again, T_c was restricted largely to temperatures which permitted thermal equilibration before onset of noticeable crystallization. At T_c = 543.2 K a small amount of crystallization occurred at lower temperature. Its melting behavior was, however, not separable from the major isothermal crystallization.

0024-9297/86/2219-1868$01.50/0

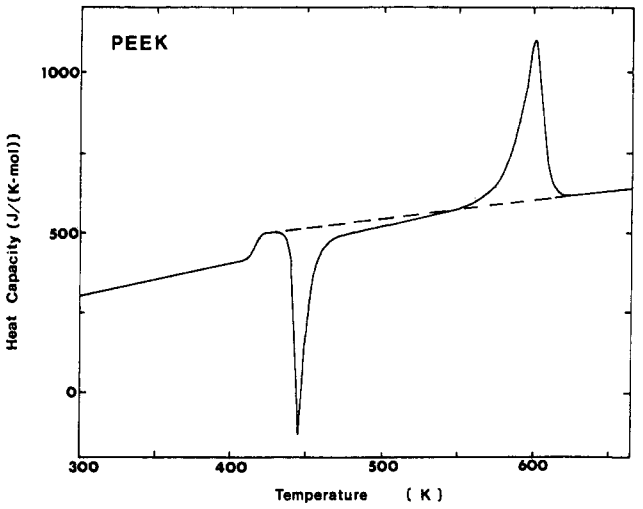

Figure 1. DSC melting trace of quenched PEEK (from the melt to liquid N_2 temperature). The glass transition temperature, T_g, is 419 K, ΔC_p at T_g is 78.1 J K^{-1} mol^{-1}, an exothermic crystallization peak can be seen at 446 K, and melting occurs at about 600 K. The heating rate is 10 K/min.

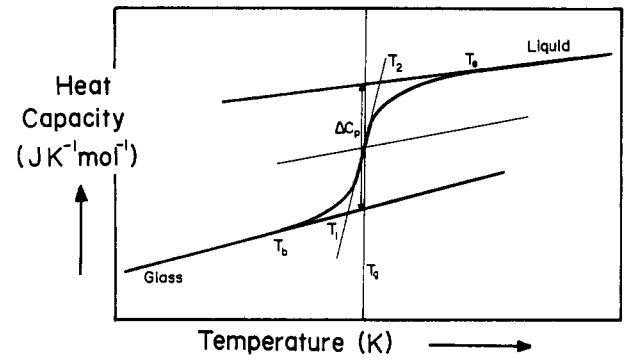

Figure 2. Schematic DSC trace in the glass transition region. For analysis, see text.

Heating rates of 0.31–40 K/min were used in some cases for the analysis of samples crystallized isothermally from both the melt and the glassy states (without cooling before analysis).

Two-step isothermal crystallization experiments were performed to get information on multiple melting peaks. The first step was crystallization at a lower T_c for a certain t_c; then, the samples were heated to a higher crystallization or annealing temperature for completion. The second temperature was chosen where the lower melting peak had been observed before. A DSC melting trace was then recorded for analysis after the sample was cooled to 325 K at −0.31 K/min.

Nonisothermal crystallization was performed at cooling rates from −0.31 K/min to −10 K/min directly from the melt after the PEEK samples were heated to 680 K and kept there for about 2 min.

The heat capacity of reproducibly produced PEEK was then measured in the four temperature ranges listed above. The two low-temperature ranges (130–250 and 220–380 K) are of importance for the discussion of heat capacity below T_g. The third range (325–500 K) allows the study of the PEEK glass transition as a function of crystallinity. Finally, the (400–650 K) region permits the analysis of the melting region.

The glass transition region is characterized by five temperatures as illustrated in Figure 2. The first perceptible beginning of the glass transition, T_b, is judged by the first increase in heat capacity from that of the solid state (glassy or crystalline). The extrapolated beginning and end of the glass transition T_1 and T_2 are indicative of the broadness of the major portion of the glass transition. The glass transition temperature T_g is chosen at half-devitrification when judged by heat capacity increase. Finally, T_e, the end of glass transition, is reached when the heat capacity reaches the liquid heat capacity. In case of hysteresis at the glass transition, its peak temperature is also recorded. The heat capacity increase ΔC_p is always chosen at T_g. For semicrystalline samples ΔC_p is sometimes not proportional to the amorphous weight fraction $(1 - w^c)$; i.e., from ΔC_p one can calculate only an overall "rigid fraction f_r" that remains solid beyond the glass transition region as analyzed in Figure 2.

$$f_r = 1 - \Delta C_p/78.1 \qquad [C_p \text{ in J K}^{-1} \text{ mol}^{-1}] \tag{1}$$

To study the hysteresis at the glass transition, the samples were heated to just above T_g and cooled at various chosen rates before analysis. Besides the peak temperature, the endothermic peak area above the liquid base line was measured for the discussion of hysteresis.

For the crystallization and melting peaks three characteristic temperatures are usually considered: the onset, the peak (maximum), and the crystallization or melting end temperatures. In this paper all crystallization and meltings are characterized by their peak temperatures. The area of the crystallization or melting peak above the heat capacity base line gives the heat of crystallization or fusion, usable for weight-fraction crystallinity determination

$$w^c = \Delta H_f/37.5 \qquad [\Delta H_f \text{ in kJ/mol}] \tag{2}$$

The two-phase crystallinity model can be applied in the temperature range T_g–T_m to the description of the thermodynamic functions if $f_r = w^c$.

Results

Heat Capacities of PEEK below T_g. In the temperature range 130–240 K the semicrystalline heat capacities agreed to better than ±0.5% with the prior established heat capacities of fully amorphous PEEK derived from the vibrational spectrum and two Tarasov Θ-temperatures, Θ_1 = 559.6 K and Θ_3 = 40 K.[1] The heat capacities measured in this research were fitted to the following two equations:

$$C_p = \exp[0.1695(\ln T)^3 - 2.193(\ln T)^2 + 10.08(\ln T) - 11.63] \tag{3}$$

in J K^{-1} mol^{-1} for five measurements on two samples at 130–200 K and with a deviation of ±2.5%.

$$C_p = 0.00005455T^2 + 1.057T + 9.631 \tag{4}$$

in J K^{-1} mol^{-1} for five measurements on two samples at 200–240 K and with a deviation of ±1.2%. Equations 3 and 4 fit the calculated heat capacity with a deviation of −0.2 ± 0.3%. Above 240 K increasing heat capacities are found for a less crystalline sample. Figure 3 shows a plot of the heat capacity as a function of the rigid fraction as determined by eq 1. At 270 K the highest rigid fraction sample (f_r = 0.6) has a 1% lower heat capacity. This increases to about 2% at 340 K and remains constant to the beginning of the major portion of the glass transition above 410 K.

Glass Transitions of Semicrystalline PEEK. The glass transition characterizations of 13 samples of different thermal history are listed in Table I. The broadness of the major glass transition region (ΔT_1) for nonisothermal crystallization increases with increasing cooling rate. It remains at 9–10 K for all isothermally crystallized samples cooled at −0.31 K/min. The width of the glass transition (ΔT_2) is high because of an increase in T_e for the samples crystallized on heating from the glassy state and increases with decreasing cooling rate in the nonisothermally crystallized samples. The beginning of the glass transition is the same for all samples (but note the additional, small heat capacity increase shown in Figure 3). The change in glass transition temperature T_g as a function of crystallization temperature T_c is shown in Figure 4. Depending on crystallization conditions, T_g changes with the lowest

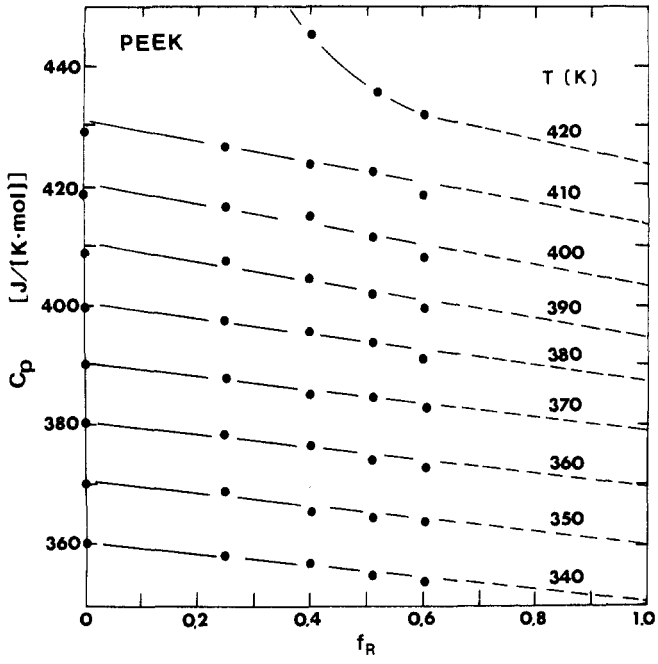

Figure 3. The dependence of heat capacity on the rigid fraction in the temperature range 340–420 K. T_g = 419 K. The highest rigid fraction sample (f_r = 0.6) was obtained by long-time annealing (annealing temperature was 603.2 K for 3 days, followed by cooling at −0.31 K/min). The second one (f_r = 0.51) is for isothermal crystallization. (T_c = 563.2 K, 2 h; see Table II). The third one (f_r = 0.40) was cooled at −80 K/min, and the fourth one (f_r = 0.23) was quenched to room temperature.

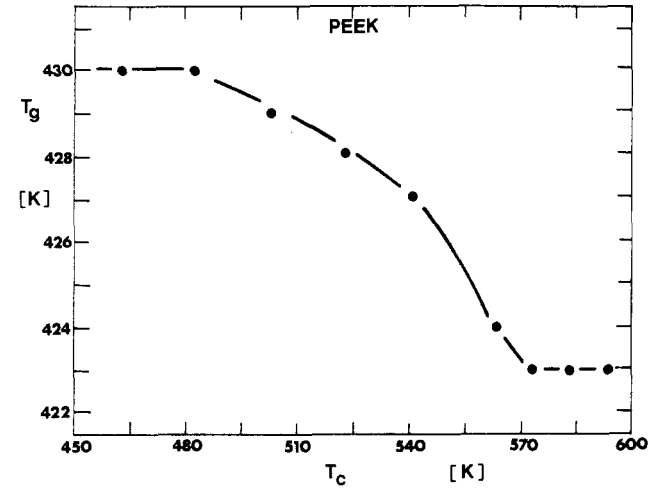

Figure 4. The relationship between glass transition T_g and isothermal crystallization temperature T_c.

crystallization temperatures, causing the largest effect. Three limiting DSC curves in the glass transition region are shown in Figure 5.

Hysteresis in the T_g Region. Figure 6 shows the hysteresis of the heat capacity of amorphous PEEK in the T_g region. The biggest endothermic hysteresis peak is Δh = 0.521 kJ/mol (cooling rate −0.31 K/min). The decrease of the endotherm with increasing cooling rate is shown in Figure 7. Finally, the quenched PEEK samples show a very small, but noticeable exothermic hysteresis peak below T_g. Comparing the crystallization exotherms, one can observe that the amorphous sample cooled slowly through T_g has a 1 K higher crystallization temperature than the quenched-only sample. Figure 8 shows, furthermore, that the crystallization exotherm peaks of samples with hysteresis (cooled slowly through T_g) show a clearly broadened crystallization with a high-temperature

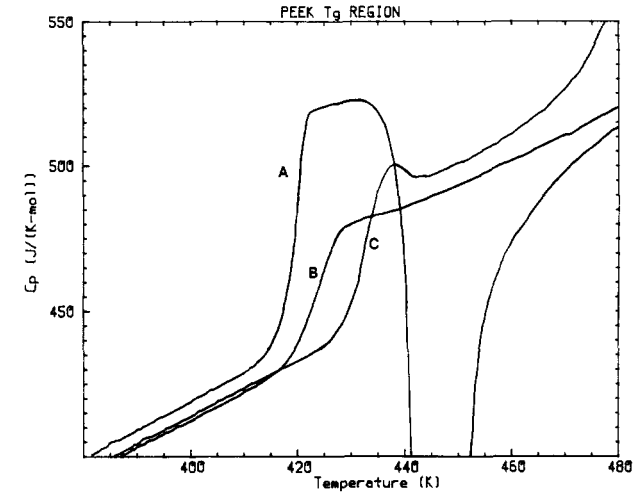

Figure 5. DSC traces of amorphous and semicrystalline PEEK in the T_g region: (A) amorphous sample; (B) isothermally melt crystallized (at 593.2 K for 24 h and then cooled to room temperature at −0.31 K/min); (C) isothermally glass-crystallized sample (463.2 K for 2 h and then cooled to room temperature at −0.31 K/min). Heating rate, 10 K/min.

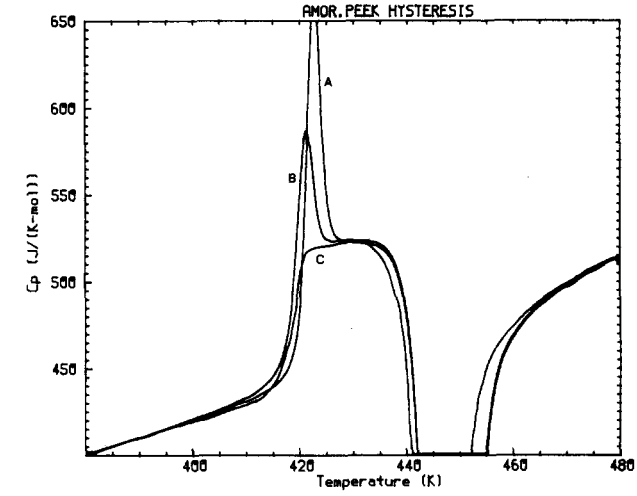

Figure 6. Hysteresis study of amorphous PEEK cooled at different cooling rates through T_g: (A) −0.31 K/min; (B) −2.5 K/min; (C) quenched to liquid N_2. Heating rate, 10 K/min.

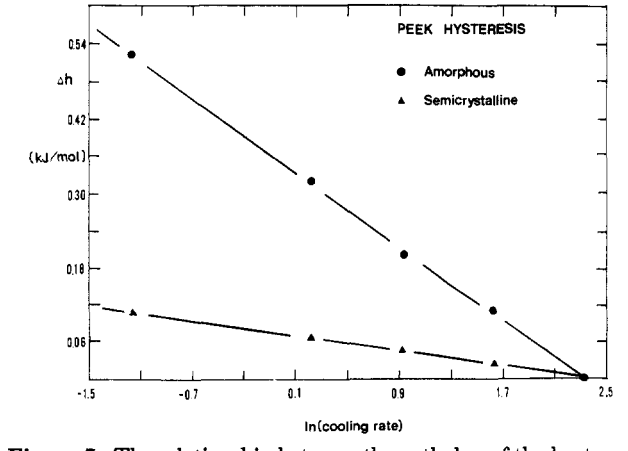

Figure 7. The relationship between the enthalpy of the hysteresis peak and the logarithmic cooling rate for both amorphous and semicrystalline PEEK. Heating rate 10 K/min (ln 10 = 2.30).

shoulder. The total crystallization peak area, however, does not seem to change.

For semicrystalline PEEK, the hysteresis effect is much less than for amorphous PEEK. Figure 7 shows a smaller endothermic hysteresis peak than expected for a slowly

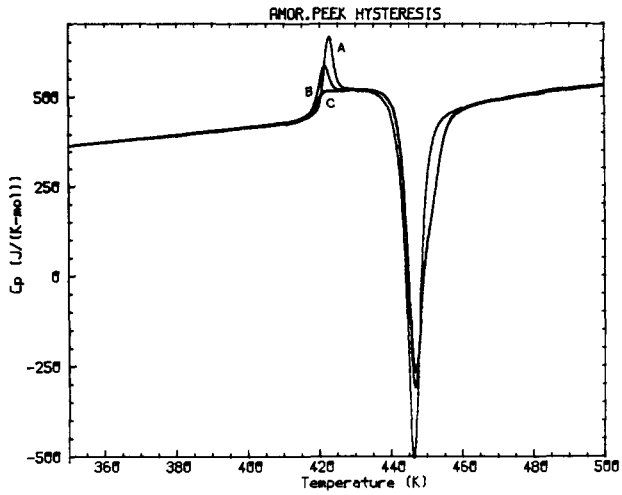

Figure 8. Hysteresis of amorphous PEEK followed by crystallization (cooling through the glass transition region: (A) –0.31 K/min; (B) –2.5 K/min; (C) quenched to liquid N_2).

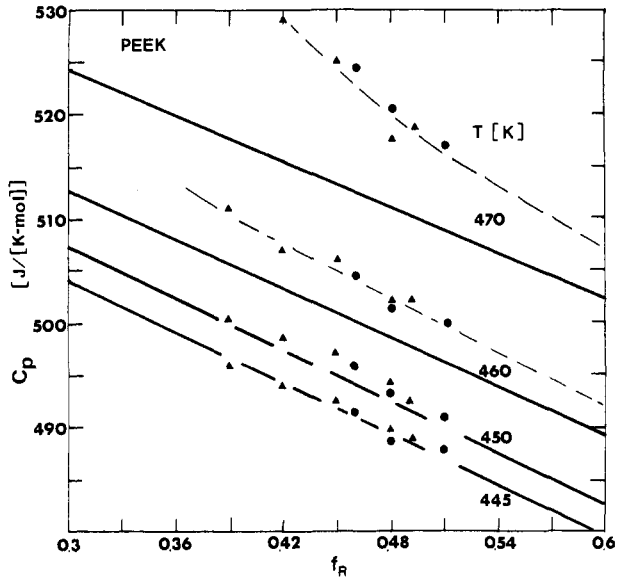

Figure 9. The rigid-fraction dependence of the heat capacity above T_g. Solid lines are calculated based on the solid and liquid heat capacity data of ref 1 and 2. Circles are for isothermal crystallization data, and triangles are for nonisothermal crystallization data.

cooled PEEK sample (–0.31 K/min, f_r = 0.50). The hysteresis peak is, in addition, considerably broadened as can be seen in Figure 5. Finally, the best crystallized sample of Figure 5 shows almost no hysteresis, despite the fact that it was cooled as slowly through T_g as curve A in Figure 6.

Heat Capacity of Semicrystalline PEEK above T_g. Heat capacity data of both solid and liquid PEEK have been reported before.[1,2] It is possible for us to study thus the semicrystalline PEEK as a function of crystallinity or rigid fraction between the glass transition temperature, T_g, and the melting transition temperature, T_m. For PEEK crystallized from the melt and the glassy state the rigid-fraction dependence of heat capacities is shown in Figure 9. The solid lines were calculated from the known solid and liquid heat capacity data and the rigid fraction of eq 1. It is obvious that above 450 K, an increasingly positive deviation is observed; i.e., the experimental heat capacity data are higher than the calculated ones. The deviation decreases with increasing rigid fraction and merges at higher temperatures into the low-temperature melting peaks (see below). For samples crystallized from the glassy state, the heat capacity drops beyond the low-temperature

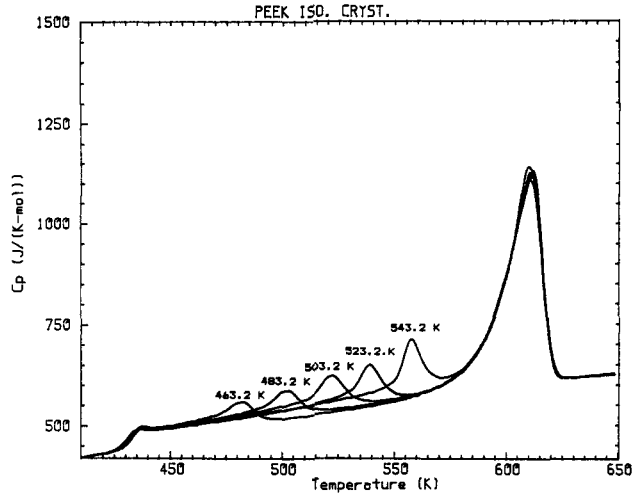

Figure 10. DSC melting traces of isothermal crystallization from the glassy state of PEEK at 463.2, 483.2, 503.2, 523.2, and 543.2 K (for 2 h for low-temperature melting peaks from left to right, respectively).

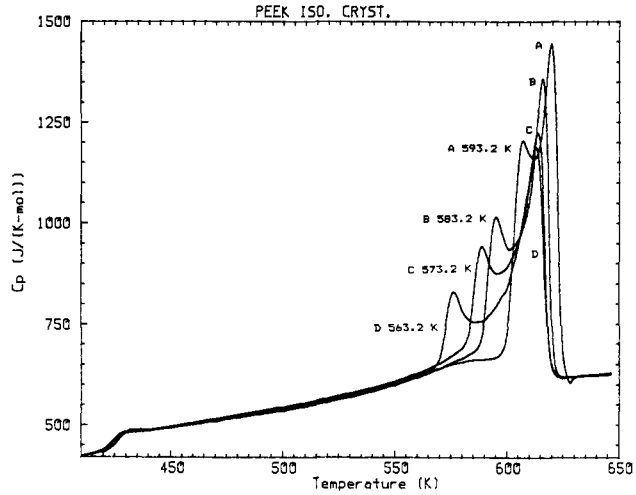

Figure 11. DSC melting traces of isothermal crystallization from the melt of PEEK at 563.2, 573.2, 583.2, and 593.2 K for 2 h for the first three samples and for 24 h for the last. (For low-melting peaks from left to right, respectively).

melting peak below that expected for the rigid fraction. For example, PEEK crystallized at T_c = 463.2 K has a rigid fraction of 44%, but its heat capacity at 500 K would correspond to f_r = 57%. This difference is outside the error limit and must be an indication of latent heat effects due to recrystallization or reorganization (see below). With increasing T_c, such negative deviation in heat capacity diminishes and turns positive, but, still, a minimum value in heat capacity can be found for all samples crystallized from the glassy state (T_c = 483.2 K at 520 K; T_c = 503.2 K at 540 K; T_c = 523.2 K at 560 K). On crystallization from the melt, the two melting peaks overlap. Their heat capacity increases continuously beyond that calculated in Figure 9 from about 460 K to the beginning of melting at about 560 K. The determination of the latent heat of fusion must thus be started for all samples at 460 K and extended to the liquid state at about 630 K; i.e., the melting range is about 170 K wide.

Relationship between T_m and T_c. Figures 10 and 11 show the DSC melting traces of semicrystalline PEEK, crystallized isothermally at different temperatures. These traces are all characterized by two melting peaks. There is a smaller, low-temperature melting peak that occurs about 15–20 K above the crystallization temperature and

Table I
Thermal Properties of PEEK in the Glass Transition Region Measured on Heating

cooling rate or T_c	T_b, K	T_1, K	T_g, K	T_2, K	T_e, K	ΔT_1, K	ΔT_2, K	ΔC_p, J K^{-1} mol^{-1}
A. Nonisothermal Crystallization on Cooling from the Melt to below T_g								
quenched	412	417	419	421	424	4	12	78.1
cooling 0.3 K/min	412	418	423	427	431	9	19	38.8
cooling 2.5 K/min	412	418	423	429	432	11	20	40.1
cooling 10 K/min	412	418	424	430	433	12	21	39.0
B. Isothermal Crystallization from the Glass, Followed by Cooling at −0.31 K/min to below T_g								
463.2 K, 2 h	412	425	430	435	445	10	33	43.7
483.2 K, 2 h	412	425	430	435	445	10	33	43.0
503.2 K, 2 h	412	424	429	434	444	10	32	42.2
523.2 K, 2 h	412	423	428	433	443	10	31	43.0
543.2 K, 2 h	412	422	427	432	442	10	30	42.0
C. Isothermal Crystallization from the Melt, Followed by Cooling at −0.31 K/min to below T_g								
563.2 K, 2 h	412	419	424	428	431	9	19	42.2
573.2 K, 2 h	412	418	423	427	430	9	18	42.2
583.2 K, 2 h	412	418	423	427	430	9	18	40.6
593.2 K, 24 h	412	418	423	427	430	9	18	38.3

Table II
Thermal Properties of PEEK in the Melting Transition Region Measured on Heating at 10 K/min

cooling rate or T_c	w^c(T)	w^c(H)	w^c(L)	w^c(I)	w^c(C)	f_r	$f_r - w^c$(T)
A. Isothermal Crystallization from the Glass and Then Cooling at −0.31 K/min							
463.2 K, 2 h	0.30	0.29	0.01	0.30	0.004	0.44	0.14
483.2 K, 2 h	0.33	0.30	0.02	0.32	0.01	0.45	0.12
503.2 K, 2 h	0.35	0.31	0.025	0.335	0.015	0.46	0.11
523.2 K, 2 h	0.35	0.30	0.03	0.33	0.02	0.45	0.10
543.2 K, 2 h	0.38	0.29	0.06	0.35	0.03	0.46	0.08
B. Isothermal Crystallization from the Melt and Then Cooling at −0.31 K/min							
563.2 K, 2 h	0.44	0.29	0.09	0.38	0.06	0.46	0.02
573.2 K, 2 h	0.46	0.26	0.12	0.38	0.08	0.46	0.0
583.2 K, 2 h	0.48	0.23	0.15	0.38	0.10	0.48	0.0
593.2 K, 24 h	0.51	0.20	0.18	0.38	0.13	0.51	0.0
C. Nonisothermal Crystallization from the Melt							
10 K/min	0.39	0.24	0.15			0.50	0.11
2.5 K/min	0.40	0.22	0.18			0.49	0.09
0.31 K/min	0.45	0.23	0.22			0.50	0.05

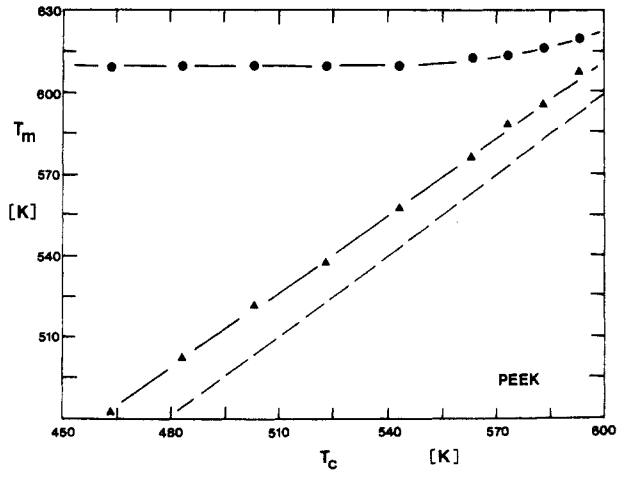

Figure 12. The relationship between T_m and T_c of PEEK. The dashed line is for $T_c = T_m$.

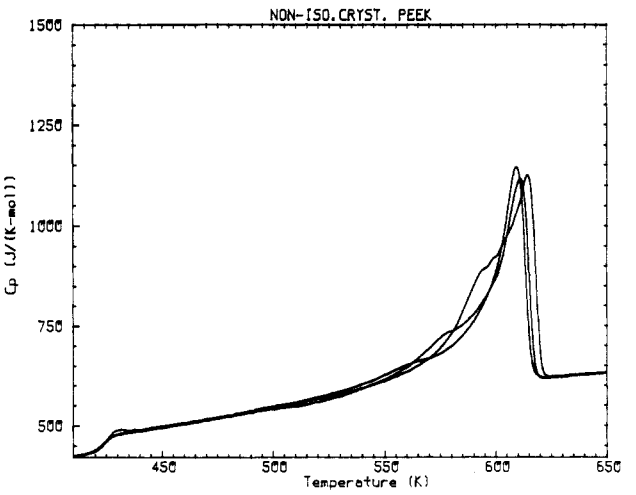

Figure 13. DSC melting traces after nonisothermal crystallization at different cooling rates (−10, −2.5, and −0.31 K/min for low-temperature melting peaks from left to right, respectively).

a larger peak that occurs above 580 K. The lower melting peak temperatures depend on the isothermal crystallization conditions. The higher melting peak temperatures are almost constant for $T_c < 563.2$ K; for $T_c > 563.2$ K, it increases somewhat with T_c. The relationship between T_m and T_c for both melting peaks is shown in Figure 12.

For nonisothermal crystallization two melting peaks are still recognizable, but less clear, as is shown in Figure 13. Again, the heat capacities start deviating from a fixed rigid fraction at about 450 K (Figure 9). Both melting peaks temperatures decrease, in this case, with increasing cooling rates.

Heat of Fusion of PEEK. The quantitative analysis of the heats of fusion for the two melting peaks shown in Figure 10 and 11 can be carried out after setting of the base line by heat capacity. The results are listed in Table II. There are three parts to the heat of fusion: that of the higher temperature melting peak, that of the lower temperature melting peak, and that set during the cooling at

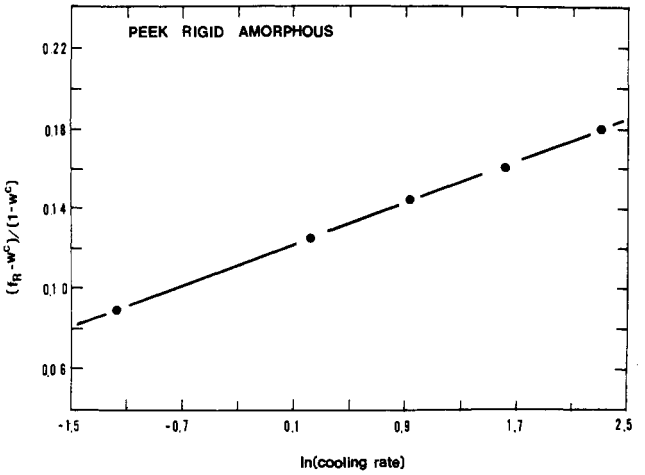

Figure 14. The relationship between $(f_r - w^c)/(1 - w^c)$ and logarithm of cooling rate.

−0.31 K/min. The last part can be determined by difference from samples analyzed with and without cooling before analysis.

For isothermal crystallization from the glassy state the total crystallinity $w^c(T)$, the crystallinity of the lower melting peak, $w^c(L)$, and the crystallinity contributed during cooling, $w^c(C)$, increase with T_c. The crystallinity indicated by the higher melting peak, $w^c(H)$, does not change very much with T_c. The values of $w^c(T)$, $w^c(L)$, and $w^c(C)$ on isothermal crystallization from the melt increase also, but $w^c(H)$ decreases. A compensation between $w^c(H)$ and $w^c(L)$ leads to an almost constant $w^c(I) = w^c(H) + w^c(L)$ (=0.38). This has been confirmed by isothermal crystallization without cooling. The values for $w^c(H)$ and $w^c(L)$ [and thus $w^c(I)$] are the same with or without cooling before analysis. The crystallinity of the isothermally melt-crystallized samples increases thus only because of additional crystallization on cooling below T_c.

Finally, a comparison between the rigid fraction from ΔC_p at T_g, f_r (eq 1), and the total crystallinity, $w^c(T)$ (eq 2) has been made. The data are listed also in Table II. On isothermal crystallization from the melt at higher T_c, f_r is equal to w^c. At lower T_c, there is a higher f_r than w^c. The difference between f_r and w^c is called the rigid-amorphous fraction. For the isothermal crystallization from the glassy state, the rigid-amorphous fraction at T_c = 463.2 K is 14%, and it decreases to 0.08 with increasing T_c.

For nonisothermal crystallization at different cooling rates, the total crystallinity, $w^c(T)$, increases with decreasing cooling rate and so does the low-melting crystallinity, $w^c(L)$. On the other hand, $w^c(H)$, the high-melting crystallinity, does not change very much (see Figure 13). These results are listed in Table II. Again, the rigid-amorphous fraction has been obtained for nonisothermal crystallization, and it increases from 5% to 11% with cooling rate (−0.31 to −10 K/min). Figure 14 shows that under such crystallization conditions 9%, 15%, and 18% of the total amorphous PEEK have a heat capacity identical with that calculated under the assumption of vibrational motion only, i.e., represent rigid-amorphous material above T_g.

Conversion between the Two Melting Peaks. Studies as to the conversion between the two melting peaks were carried out. Different heating rates have been used for analysis after isothermal crystallization without cooling. The results are listed in Table III. One can find that for the three chosen crystallization temperatures the crystallinity of the lower melting peak, $w^c(L)$, decreases with heating rate. Correspondingly, the crystallinity of the higher melting peak, $w^c(H)$, increases, so that the total crystallinity obtained during the isothermal crystallization is constant. Figure 15 shows a plot of the crystallinity, $w^c(L)$, and the logarithmic heating rate.

Table III
Crystallinities of the Melting Peaks at Different Crystallization Temperatures and Heating Rates

heating rate, K/min	$w^c(L)$	$w^c(H)$	$w^c(I)$
	T_c = 523.2 K		
2.5	0.02	0.31	0.33
10	0.03	0.30	0.33
20	0.04	0.29	0.33
40	0.045	0.28	0.32
	T_c = 573.2 K		
0.31	0.05	0.33	0.38
2.5	0.09	0.29	0.38
10	0.12	0.26	0.38
40	0.14	0.24	0.38
	T_c = 593.2 K		
0.31	0.11	0.27	0.38
2.5	0.15	0.23	0.38
10	0.18	0.20	0.38

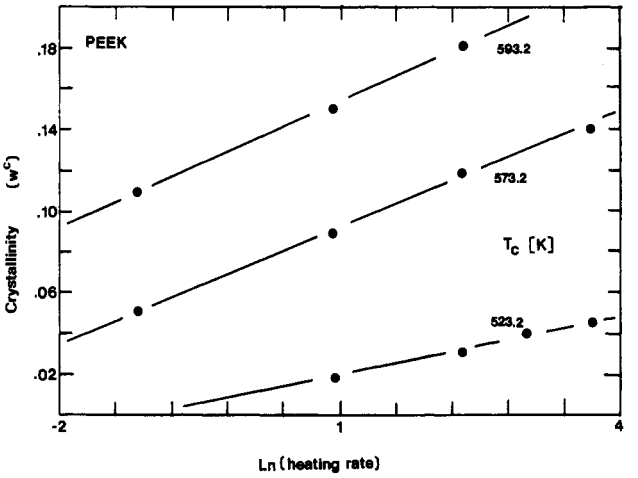

Figure 15. The relationship between the lower melting peak crystallinity $w^c(L)$ and logarithmic heating rate (in K/min).

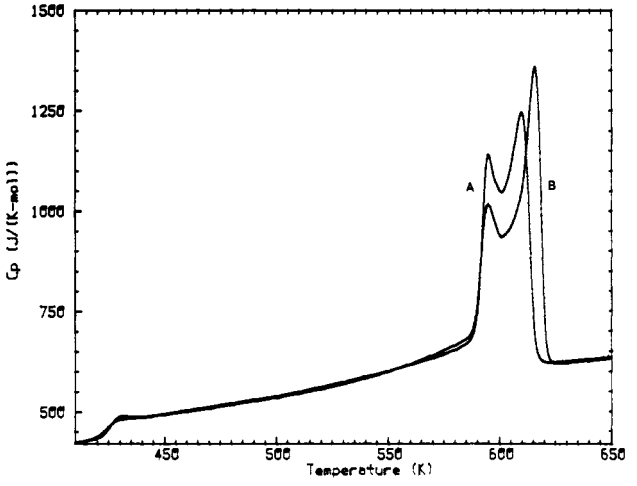

Figure 16. Two-step isothermal crystallization from the melt. Curve A: T_c = 563.2 K, held 2 h, heated to 583.2 K at 10 K/min, held there 2 h, and cooled down to room temperature at −0.31 K/min before recording. Curve B: one-step, isothermal crystallization from the melt (T_c = 583.2 K, held 2 h, and cooled down to room temperature at −0.31 K/min before recording).

Melting of Samples Crystallized Isothermally in Two Steps. Figures 16 and 17 show DSC melting traces for the two-step isothermal crystallizations. Superficially

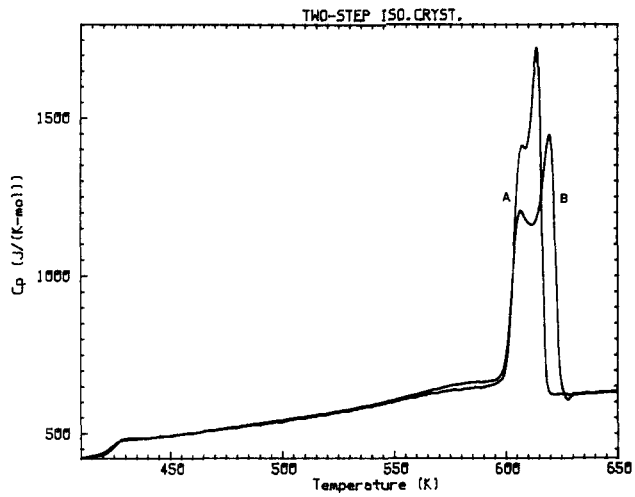

Figure 17. Two-step isothermal crystallization from the melt. Curve A: T_c = 573.2 K, held 2 h, heated to 593.2 K at 10 K/min, held there 24 h, and cooled down to room temperature at −0.31 K/min before recording. Curve B: one-step isothermal crystallization from the melt. (T_c = 593.2 K, held 24 h, cooled down to room temperature at −0.31 K/min before recording).

Table IV
Comparison of Thermal Properties Obtained by One-Step and Two-Step Isothermal Crystallizations

T_c, K, and t_c,[a] h	T_g, K	T_m, L	T_m, H	w^c(T)	f_r = w^c(T)
Crystallization A					
463.2, 2 h	430	482	610	0.30	0.14
503.2, 2 h	429	522	610	0.35	0.11
463.2, 2 h, 503.2, 2 h	429	522	610	0.35	0.12
Crystallization B					
503.2, 2 h	429	522	610	0.35	0.11
543.2, 2 h	427	558	610	0.38	0.08
503.2, 2 h, 543.2, 2 h	427	558	610	0.38	0.08
Crystallization C					
563.2, 2 h	424	576	612	0.44	0.02
583.2, 2 h	423	595	616	0.48	0.00
563.2, 2 h, 583.2, 2 h	423	595	612	0.48	0.00
Crystallization D					
573.2, 2 h	423	588	613	0.46	0.00
593.2, 24 h	423	607	620	0.51	0.00
573.2, 2 h, 593.2, 24 h	423	607	613	0.52	0.00

[a] Single temperature and time express one-step isothermal crystallization condition; double temperatures and times express two-step isothermal crystallization conditions.

they correspond to the normal (one-step) isothermal crystallizations. Quantitatively, however, one finds the lower melting peak temperatures to correspond to those of the one-step, isothermal crystallizations at the higher of the two-step crystallization. The higher melting peak temperature, in contrast, is always that fixed at the first step of the crystallization; i.e., there is a "memory effect".

The two-step crystallinities w^c(L) and w^c(H) are changed from the one-step values, but w^c(T) and w^c(I) increase only very little (<1%). For example, in Figure 16, the crystallinity of the lower melting peak, w^c(L), is 18%, 3% higher than for one-step isothermal crystallization at T_c = 583.2 K and 9% higher than for one-step isothermal crystallization at T_c = 563.2 K. That of the higher melting peak, w^c(H), is 20%, 3% lower than for one-step crystallization at T_c = 583.2 K and 9% lower than for one-step isothermal crystallization at T_c = 563.2 K. The detailed analyses are listed in Table IV.

Sequence of Crystallization. To establish the sequence of crystallization of PEEK, isothermal crystallizations at 583.2 K were interrupted at different crystallization times. The immediate analyses after different times t_c are shown in Figure 18. After 1.8 min there is still no observable crystallization and then a broad-melting, high-temperature crystallinity develops w^c(H). With time the melting peak gets sharper and a distinct low-temperature crystallinity w^c(L) can be seen after about 10 min. The ratio w^c(L) to w^c(H) increases with time, and both peaks move to slightly higher melting temperature as crystallization proceeds.

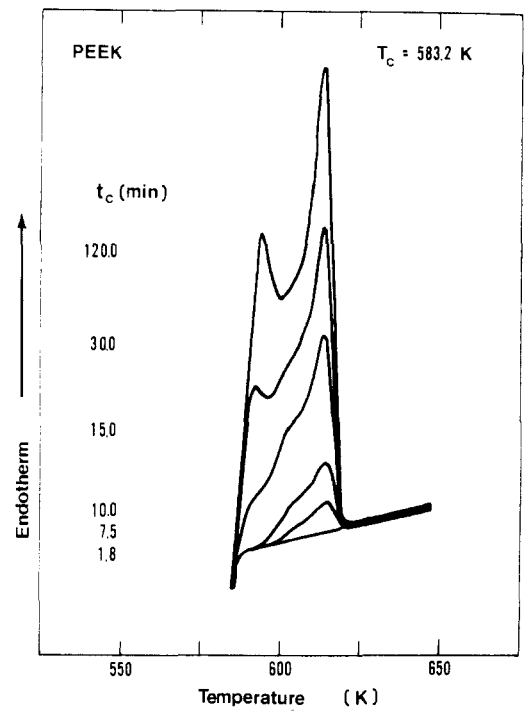

Figure 18. Analysis of crystals grown at 583.2 K for different lengths of time. The flat base line after 1.8-min crystallization shows no crystallization.

Discussion

Heat Capacity below T_g. Below 240 K the heat capacities of all samples of different crystallinity agreed within experimental error. Such independence of C_p on crystallinity has been observed also for other polymers.[17]

Above 240 K there is a slight dependence of heat capacity on crystallinity or rigid fraction, as shown in Figure 3. An often considered cause for such increase in heat capacity with increasing amorphous content may be the local modes of motion[18] still active below T_g. It may also be possible that because of the high glass transition temperature of PEEK a larger $C_p - C_v$ for the glass can account for the increase in C_p. This difference $C_p - C_v$ can be approximated by the Lindemann equation

$$C_p - C_v = A_0 C_p^2 T / T_m \quad (5)$$

where A_0 is a constant and T_m is the melting temperature, or the exact thermodynamic relationship

$$C_p - C_v = TV\alpha^2/\beta \quad (6)$$

where α is the expansivity and β the compressibility. Indeed, other polymers of high glass transitions such as polycarbonates[19] and poly(ethylene terephthalate)[20] seem to have similar, small positive heat capacity contributions for the glass.

Possible local motions below T_g have been identified by dynamic mechanical analysis. Some degree of rotation of the phenylene and ketone groups was linked in the glass to the γ-relaxation which starts at about 197 K, molecular

local motion of aligned and oriented chain segments was suggested to occur at 233 K, and finally, a β'-relaxation at 313K was related to main chain mobility.[21]

A quantitative link of the heat capacity increase of glasses below T_g to motion, as was possible for polyethylene,[22] could not be developed for PEEK.

Glass Transition of Semicrystalline PEEK. Table I and Figures 1 and 5 show that the quenched PEEK has the sharpest and largest glass transition. The observed ΔC_p of 78.1 J K^{-1} mol^{-1} is in agreement with the empirical rules of increase in heat capacity at T_g.[2] Any crystallization broadens the glass transition range and shifts its end, T_e, to higher temperature by as much as 20 K. The glass transition temperature, T_g, itself is shifted by at most 11 K (all at 10 K/min heating rate). As the crystallization becomes more restrictive (i.e., the faster the cooling rate on nonisothermal cooling or the lower the crystallization temperature on isothermal crystallization from the melt), the effect becomes greater. Figure 4 shows the range of T_g as a function of crystallization temperature. Coupled with this broadening of the glass transition range to higher temperatures is an increase in the rigid-amorphous PEEK above T_g (Table II and Figure 14). For the crystallization at 463.2 K it reaches 20% of the remaining amorphous portion (70%). On high-temperature crystallization there is no rigid-amorphous fraction.

Observations of crystal morphology[3,7] have revealed differences in the crystallization regions of varying amorphous fractions. Low nucleation rate (large spherulites) and more perfect cylindrically aggregated lamellar crystals are observed at high crystallization temperature. At lower T_c higher nucleation density and more random lamellae are observed. It seems logical that smaller and less perfect lamellae increase the amount of material at the crystalline–amorphous interface and also increase the residual strain at the interface.

Similar rigid-amorphous parts in polymers were observed in poly(oxymethylene)[24] and polypropylene.[25] Of these two examples one could not discover a separate glass transition for poly(oxymethylene); i.e., the rigid-amorphous fraction became mobile only in the melting region. Polypropylene, in contrast, has a rigid-amorphous fraction that decreases continuously and becomes zero just before melting. In the present case the analysis of the possible change in rigid-amorphous material with temperature is complicated by the early melting of PEEK with high rigid-amorphous fractions. Figure 9 shows that at least up to 450 K there is no indication of a change in amorphous fraction. A possible glass transition of the amorphous fraction at 460 K or above merges with the lower temperature fusion.

Hysteresis in the T_g Region. Figure 6 shows that amorphous PEEK shows typical hysteresis in heat capacity when a slowly cooled sample is heated quickly. A series of other polymers were analyzed earlier[26,27] and showed a similar behavior as a function of cooling rate. Of special interest is the fact that the hysteresis of semicrystalline samples is reduced by more than expected from the rigid fraction (see Figures 7 and 5). Also, the broadening of the glass transition region (Table I) is not sufficient to explain the decreased hysteresis. The crystal–amorphous interface must reduce the time dependence of the glass transition, as was found recently for other semicrystalline polymers such as poly(ethylene terephthalate).[28]

The change in the structure of the glass on slower cooling through T_g is also revealed by a changed crystallization behavior (Figure 8). The sample cooled slowly through the glass transition does not crystallize faster, but slower. Since nucleation is often related only to time at sufficiently low temperature, one may speculate that the change in crystallization is due to a change in glass structure which has not fully equilibrated at the beginning of the exotherm.

A final point of interest is the small exotherm at 400–410 K of the fast-quenched sample seen in Figure 6, expected on theoretical grounds.[26] As observed for polystyrene, the exotherm seems much smaller than predicted.

Fusion of PEEK. The fusion process of PEEK is strongly dependent on the crystallization history. Technological application of the polymer will require thus a carefully controlled thermal history. As shown in this paper, thermal analysis seems able to quickly analyze the crystals present in the sample.

Table II and Figures 10, 11, 16, and 17 reveal that three different crystallinities must be identified: (1) the high-melting and usually major portion, w^c(H); (2) the low-melting portion, w^c(L); (3) a broad portion crystallized on cooling w^c(C). The development of crystallinity of Figure 18 indicates that the high-melting crystals grow first, followed by the low-melting fraction. The high-melting fraction seems to develop out of an intermediate fraction as was observed prior for polyethylene.[29] The fact that increasing heating rates increase the ratio of low- to high-melting crystallinity (Table III and Figure 15) shows that the low-melting crystals reorganize to some degree and can, at sufficiently high temperature, become part of the high-melting crystals. At sufficiently low temperature, this reorganization becomes possibly, as shown in Figure 10, a recrystallization with an exothermic contribution to the heat capacity.

The two-step crystallizations (Figures 16 and 17, Table IV) show also that (1) not as much high-melting crystallinity w^c(H) is produced at T_c (at least $^1/_3$ less at 563.2 K) as is formed on heating; i.e., reorganization and recrystallization must account for the difference (see also Figure 15); (2) the low-melting crystallinity w^c(L) accounts for most of the rigid-amorphous fraction (and shift in T_g) and its true fraction is larger than indicated by w^c(L); (3) the perfection of the low-melting crystals on heating is limited by the already present high-melting crystals.

On continuous cooling for crystallization (Figure 13) the different crystallization stages are less visible. The T_m/T_c plot (Figure 12) shows the typical polymer behavior.[13] The low-melting peak is similar to the typical "annealing peak",[13] and the high-melting peak stays constant for a wide crystallization temperature; it sets also the limit of reorganization. Only at the highest crystallization temperatures is an increase in T_m of the high-melting crystals toward the equilibrium melting temperature noticeable, which was projected to be 668 K from melting temperature vs. lamellar (low-angle X-ray) thickness correlation.[3]

The additional crystallinity developed on cooling after completion of crystal growth at T_c, w^c(C), increases continuously with T_c and accounts for the major change in w^c(T) with T_c. It must represent crystals of low perfection. In fact, there is a close correlation between these crystals grown on cooling and the rigid-amorphous fraction. When fewer of these crystals are grown, the rigid-amorphous fraction is higher (see Table II); i.e., the total rigid fraction f_r (eq 1) does not vary substantially (0.44–0.51) with the isothermal crystallization conditions in the research, although other conditions might be found to accomplish bigger changes (annealing, quick cooling, etc.; see also Figure 3).

Conclusions

In a thermal analysis of PEEK it is necessary to specify three types of crystallinity w^c(H), w^c(L), and w^c(C) and the

rigid-amorphous fraction. Not only must the glass transition be characterized by T_g but also information on its breadth and hysteresis is valuable to specify strain on the amorphous portions. Such detailed analysis is possible by separation of the heat capacity known from independent analysis from the overall thermal effects. All of the crystals (and the rigid-amorphous fraction) are metastable, and their change during analysis due to reorganization, perfection, and recrystallization must be assessed. A slightly higher heat capacity at constant pressure of amorphous PEEK below T_g cannot be fully assigned at present.

Much further work, especially on the time dependence of crystallization and annealing as well as on different crystallization conditions, is possible to reach the degree of specification needed for reproducible and reliable application of PEEK as composite matrix.

Acknowledgment. This research was supported by a NASA Institute Grant No. NGL32-018-003 and by the National Science Foundation, Polymers Program, Grant No. DMR 83-17097.

Registry No. PEEK, 31694-16-3.

References and Notes

(1) Cheng, S. Z. D.; Lim, S.; Judovits, L.; Wunderlich, B. *Polymer* to be published.
(2) Cheng, S. Z. D.; Wunderlich, B. *J. Polym. Sci., Polym. Phys. Ed.*, to be published.
(3) Blundell, D. J.; Osborn, B. N. *Polymer* **1983**, *24*, 953.
(4) Dawson, P. C.; Blundell, D. J. *Polymer* **1980**, *21*, 577.
(5) Rueda, D. R.; Ania, F.; Richardson, A.; Ward, I. M.; Balta Calleja, F. J. *Polym. Commun.* **1983**, *24*, 258.
(6) Wakely, N. T. *Polym. Commun.* **1984**, *25*, 306.
(7) Lovinger, A. J.; Davis, D. D. *J. Appl. Phys.* **1985**, *58*, 2843.
(8) Lovinger, A. J.; Davis, D. D. *Polym. Commun.* **1985**, *26*, 322.
(9) Attwood, T. E.; Dawson, P. C.; Freeman, J. L.; Hoy, L. R.; Rose, J. B.; Staniland, P. A. *Polymer* **1981**, *22*, 1096.
(10) Bishop, M. T.; Karasz, F. E.; Russo, F. E.; Langley, K. H. *Macromolecules* **1985**, *18*, 86.
(11) Gaur, U.; Wunderlich, B. *Macromolecules* **1980**, *13*, 445.
(12) Suzuki, H.; Wunderlich, B. *Makromol. Chem.* **1985**, *189*, 1109.
(13) Wunderlich, B. *Macromolecular Physics, Crystal Melting*; Academic: New York, 1980; Vol. III.
(14) Wunderlich, B. In *Thermal Analysis in Polymer Characterization*; Turi, E., Ed.; Wiley/Heyden: New York, 1981; p 1. See also: Wunderlich, B.; Menczel, J. *Prog. Calorimetry Thermal Anal.* **1984**, *2*, 81.
(15) Wunderlich, B.; Bopp, R. C. *J. Thermal Anal.* **1974**, *6*, 335. See also: Mehta, A.; Bopp, R. C.; Gaur, U.; Wunderlich, B. *J. Thermal Anal.* **1978**, *13*, 197.
(16) Ginnings, D. C.; Furukawa, G. T. *J. Am. Chem. Soc.* **1953**, *75*, 522.
(17) See, for example; Wunderlich, B.; Baur, H. *Adv. Polym. Sci.* **1970**, *7*, 151.
(18) Ferry, J. D. *Viscoelastic Properties of Polymers* , 3rd ed.; Wiley: New York, 1980.
(19) Cheng, S. Z. D.; Wunderlich, B., to be submitted.
(20) Gaur, U.; Lau, S.-F.; Wunderlich, B. *J. Phys. Chem. Ref. Data* **1983**, *12*, 91.
(21) Sasuga, T.; Hagiwara, M. *Polymer* **1985**, *26*, 501.
(22) Wunderlich, B. *J. Chem. Phys.* **1962**, *37*, 2429.
(23) Wunderlich, B. *Macromolecular Physics, Crystal Nucleation, Growth, Annealing*; Academic: New York, 1976; Vol. II.
(24) Suzuki, H.; Wunderlich, B. *Makromol. Chem.* **1985**, *189*, 1109.
(25) Grebowicz, J.; Lau, S. F.; Wunderlich, B. *J. Polym. Sci., Polym. Symp.* **1984**, *71*, 19.
(26) Wunderlich, B.; Bodily, D. M.; Kaplan, M. H. *J. Appl. Phys.* **1964**, *35*, 95.
(27) Wolpert, S. M.; Weitz, A.; Wunderlich, B. *J. Polym. Sci., Part A-2* **1971**, *9*, 1887.
(28) Menczel, J.; Wunderlich, B. *J. Polym. Sci., Polym. Lett. Ed.* **1981**, *19*, 261.
(29) Wunderlich, B.; Melillo, L.; Cormier, C. M.; Davidson, T.; Snyder, G. *J. Macromol. Sci., Phys.* **1967**, *B1*, 485.

Complex Molecular Motions in Bulk Hard-Segment Polyurethanes: A Deuterium NMR Study

Agustin Kintanar and Lynn W. Jelinski*
AT&T Bell Laboratories, Murray Hill, New Jersey 07974
Irena Gancarz and Jeffrey T. Koberstein
Department of Chemical Engineering, Princeton University, Princeton, New Jersey 08544.
Received September 25, 1985; Revised Manuscript Received April 23, 1986

ABSTRACT: Solid-state deuterium NMR spectroscopy is used to characterize molecular motion in two specifically deuterated polyurethane hard-segment polymers. The polyurethanes consist of bis(4-isocyanophenyl)methane (MDI), chain extended with butanediol-2,2,3,3-d_4 (BDO), and 2,4-toluenediyl diisocyanate (TDI), chain extended with butanediol-2,2,3,3-d_4. Line shape and relaxation (T_1) data were obtained as a function of temperature. The results indicate a broad distribution of motional correlation times in both materials. In the semicrystalline MDI–BDO polymer, the distribution divides cleanly into two components that are attributable to the crystalline and amorphous regions of the material. In the TDI–BDO polymer, there is only a single broad distribution, in keeping with the completely amorphous nature of this material. The results also show that the predominant large-scale motion of the alkyl chain is a gauche–trans conformational hop. The central methylene carbons of the butanediol undergo librations about their equilibrium positions, in addition to the large-scale conformational transitions. Above ~60 °C, additional larger scale diffusion of the entire butanediol moiety occurs within a cone of semiangle ~15°. The results are consistent with the existence of kinked conformations in the alkyl chain of this material.

The morphology and physical properties of polyurethane block copolymers have been areas of considerable interest for at least 20 years. Studies of these thermoplastic elastomers have focused primarily on the microphase separation of the hard and soft segments into domains, to which the unique properties of these materials may be directly ascribed.

We have recently demonstrated the viability of solid-state deuterium (^{2}H) NMR as a technique for evaluating phase separation and phase mixing in polyurethanes[1] and in another segmented copolymer system, the Hytrel copolyesters.[2,3] The NMR method is based on differential segmental mobilities of ^{2}H-labeled moieties in the hard and soft domains and at the domain interfaces.

Solid-state ^{2}H NMR is a powerful tool for characterizing molecular motion in polymers.[4,5] In a rigid lattice powder, where the orientation of a selected C–D bond is random and the motions of this bond are slow on the ^{2}H NMR time

0024-9297/86/2219-1876$01.50/0